





# From response functions to cross sections in neutrino scattering off the deuteron and trinucleons

J. Golak , R. Skibiński, K. Topolnicki, H. Witała , and A. Grassi  
*M. Smoluchowski Institute of Physics, Jagiellonian University, PL-30348 Kraków, Poland*

H. Kamada   
*Department of Physics, Faculty of Engineering, Kyushu Institute of Technology, Kitakyushu 804-8550, Japan*

L. E. Marcucci  
*Department of Physics, University of Pisa, IT-56127 Pisa, Italy and INFN-Pisa, IT-56127 Pisa, Italy*

 (Received 23 August 2019; revised manuscript received 16 November 2019; published 26 December 2019)

Response functions, differential cross sections, and total cross sections for several (anti)neutrino induced reactions on  ${}^2\text{H}$ ,  ${}^3\text{He}$ , and  ${}^3\text{H}$  are calculated in momentum space for (anti)neutrino energies up to 160 MeV, using the AV18 nucleon-nucleon potential and a single-nucleon weak current operator. This work is a continuation of our earlier investigations [J. Golak *et al.*, *Phys. Rev. C* **98**, 015501 (2018)].

DOI: [10.1103/PhysRevC.100.064003](https://doi.org/10.1103/PhysRevC.100.064003)

## I. INTRODUCTION

Neutrinos interactions with atomic nuclei are important not only for nuclear physics but also for other domains like particle physics and astrophysics. Nuclei serve as neutrino detectors in experiments focusing on neutrino properties, such as oscillation measurements, as well as in experiments where neutrinos from the interior of stars or from supernova explosions carry important information. That is why a deep understanding of neutrino induced processes on nuclei is necessary for both the interpretation of current experiments and the planning of new undertakings [1,2]. For example, the use of the deuteron in heavy water detectors in the Sudbury Neutrino Observatory (SNO) for solar neutrinos motivated the theoretical efforts by Nakamura *et al.* [3,4], Shen *et al.* [5], and Baroni and Schiavilla [6] to provide accurate predictions for inclusive neutrino scattering off the deuteron.

The results of Ref. [3], a large part of the results given in Ref. [4], and the more recent predictions in [5] were obtained within the so-called standard nuclear physics approach [7], using the AV18 nucleon-nucleon (NN) force [8] and augmenting the single-nucleon current with two-nucleon (2N) contributions linked to this potential. The latest calculations in this group, by Baroni and Schiavilla [6], were in contrast fully based on chiral effective field theory ( $\chi$ EFT) input. The results of all these calculations performed in coordinate space were quite similar, which suggested that the theoretical predictions had a very small uncertainty in the low-energy neutrino regime.

We could confirm these findings by performing independent calculations in momentum space [9]. Namely, we investigated 2N and three-nucleon (3N) reactions with (anti)neutrinos in the framework very close to the one of Ref. [5] but with the single-nucleon current operator. For all the studied reactions on the deuteron, we presented results for

the total cross sections, however, we restricted ourselves to the lower (anti)neutrino energies. We found that the few percent deviations between our strictly nonrelativistic results and the predictions presented in Ref. [5] originate from the relativistic kinematics, especially the phase space factor, employed in Ref. [5]. Thus our calculations for the reactions with the deuteron passed a necessary test before we embarked on 3N calculations.

In Ref. [9] we collected important references, which dealt with calculations for neutrino scattering on heavier than  $A = 2$  nuclei and related processes like muon capture or the triton  $\beta$  decay [10–17]. Here we mention only early calculations of the  $\bar{\nu}_e + {}^3\text{He} \rightarrow e^+ + {}^3\text{H}$  and  $\bar{\nu}_\mu + {}^3\text{He} \rightarrow \mu^+ + {}^3\text{H}$  processes by Mintz *et al.*, who used an elementary particle model [18] dealing with nonbreakup reactions, and especially work by Gazit *et al.*, who performed a number of calculations for neutrino induced breakup reactions with the  ${}^3\text{H}$ ,  ${}^3\text{He}$ , and  ${}^4\text{He}$  nuclei [19–21], in which final-state interactions were included via the Lorentz integral transform method [22]. Heavier light nuclei, including  ${}^{12}\text{C}$ , were investigated with the Green's function Monte Carlo method [23–25] and using an extended factorization scheme in the spectral function formalism [26].

Our calculations in Ref. [9] for the (anti)neutrino- ${}^3\text{He}$  and (anti)neutrino- ${}^3\text{H}$  inelastic scattering were limited only to examples of the essential nuclear response functions; we did not calculate any total cross sections. In the present paper we continue our work for the (anti)neutrino reactions with the trinucleons. Within the same framework, described in Ref. [9], we performed several thousand Faddeev calculations to gather information necessary to compute the differential (with respect to the lepton arm) and total cross sections. This information was stored in the form of the response functions calculated on a sufficiently dense two-dimensional grid defined by the internal nuclear energy and the magnitude of the three-momentum transfer. The very time consuming

calculations of the response functions allowed us later to calculate, essentially in no time at all, other observables of interest. To this end simple two-dimensional interpolations were used. This method was of course first carefully tested for the reactions on the deuteron, where the results of the direct calculations exist and only then applied to the trinucleons. The results of our calculations are available upon request.

The paper is organized in the following way. Since we defined all the elements of our formalism in Ref. [9], in Sec. II we restate only crucial definitions and provide the connection between the response functions and the cross sections. In Secs. III and IV we show selected results for neutrino reactions on the deuteron and the trinucleons. In particular we discuss the properties of the 2N and 3N weak response functions and the resulting differential and total cross sections. Finally, Sec. V contains concluding remarks and outlook.

## II. CROSS SECTIONS AND RESPONSE FUNCTIONS

Our treatment of the kinematics of the  ${}^2\text{H}$ ,  ${}^3\text{He}$ , and  ${}^3\text{H}$  (anti)neutrino induced disintegration processes is the same. We start from the exact relativistic form of the energy and momentum conservation laws but later we employ nonrelativistic formulas in the nuclear sector, consistent with our nonrelativistic 2N and 3N dynamics. Here we restrict ourselves to initial (anti)neutrino energies  $E \leq 160$  MeV and we have found for all the considered reactions a very small difference (not exceeding 1 %) between the results for kinematical quantities based on the exact relativistic formulas and their approximate nonrelativistic analogs.

For a given initial (anti)neutrino energy  $E$  and a final lepton scattering angle  $\theta$ , we calculate the range of the outgoing lepton energies  $E'$  and express the internal energy of the nuclear system  $E_{\text{c.m.}}$  in terms of  $E$ ,  $\theta$ , and  $E'$ . This information is necessary to evaluate the differential and total cross sections for the (anti)neutrino induced disintegration processes. In the following the initial (anti)neutrino and final lepton momenta are denoted as  $\mathbf{k}$  and  $\mathbf{k}'$ , respectively.

The formalism of neutrino scattering off nuclei is well established; see, for example, Ref. [27]. For the charged-current (CC) induced processes it stems directly from the Fermi theory but it has to be modified to include additionally the neutral-current (NC) based processes. For the lowest order processes the transition matrix element can be written as a contraction of the nuclear part  $N^\lambda$  and the leptonic part  $L_\lambda$ , where the latter is expressed in terms of the Dirac spinors and gamma matrices in a standard way [9]. Therefore, we focus on the matrix elements

$$N^\lambda = \langle \Psi_f \mathbf{P}_f m_f | j^\lambda | \Psi_i \mathbf{P}_i m_i \rangle \quad (2.1)$$

of the nuclear weak charged or neutral current  $j^\lambda$  between the initial  $|\Psi_i\rangle$  and final  $|\Psi_f\rangle$  nuclear states, where the total initial (final) nuclear three-momentum is denoted by  $\mathbf{P}_i$  ( $\mathbf{P}_f$ ),  $m_i$  is the initial nucleus spin projection, and  $m_f$  is the set of spin projections in the final state. We evaluate the crucial nuclear matrix elements  $N^\lambda$  in momentum space and all information about our framework can be found in Ref. [9] and in references therein. Our predictions for all the CC induced

reactions are prepared only for the electron flavor. However, for the NC reactions, results are the same for all three flavors.

We assume a system of coordinates where the three-momentum transfer,  $\mathbf{Q} \equiv \mathbf{k} - \mathbf{k}'$ , is parallel to the (quantization)  $z$  axis and use the spherical components for  $N^\lambda$ . The standard steps lead to the final form of the cross section

$$\frac{d^3\sigma}{dE' d\Omega'} = \frac{G_F^2 \cos^2 \theta_C}{(2\pi)^2} F(Z, E') \frac{|\mathbf{k}'|}{8E} (V_{00}R_{00} + V_{MM}R_{MM} + V_{PP}R_{PP} + V_{ZZ}R_{ZZ} + V_{Z0}R_{Z0}), \quad (2.2)$$

where the notation in Eq. (2.2) is the same as in Ref. [9].

While the  $V_{ij}$  functions arise from the analytically known leptonic arm [9], the nuclear response functions, which are the essential dynamical ingredients in Eq. (2.2), originate from the integration of various products of the nuclear matrix elements over the whole nuclear phase space available for the fixed final lepton momentum:

$$R_{AB} = \sum_{m_i, m_f} \int df \delta(E_{\text{c.m.}} - E_f) \langle \Psi_f \mathbf{P}_f m_f | j^A | \Psi_i \mathbf{P}_i m_i \rangle \times (\langle \Psi_f \mathbf{P}_f m_f | j^B | \Psi_i \mathbf{P}_i m_i \rangle)^*. \quad (2.3)$$

The labels  $AB = 00, MM, PP, ZZ$ , and  $Z0$  stem from the various components of the current operator, and the  $df$  integral denotes the sum and the integration over all final nuclear states with the fixed internal energy  $E_{\text{c.m.}} = E_{2\text{N}}$  or  $E_{\text{c.m.}} = E_{3\text{N}}$ . The direct integration would allow one to evaluate contributions from any part of the phase space. In particular, for the reactions on  ${}^3\text{He}$  and  ${}^3\text{H}$  it would be possible to obtain contributions from the two- and three-body breakup channels. However, the numerical cost of such calculations needed for the total cross section, which is the main objective of the present paper, is very high. Thus we decided to compute the 3N response functions in a much more economical way, using closure and employing the special Faddeev scheme [28,29]. In Ref. [9] we compared results based on these two quite different approaches and found a very good agreement. The results for all the 3N response functions presented in this paper are obtained with the second, faster method. This closure-based scheme could be formulated also for the 2N system but in that case the integration over the phase space is well under control and perfectly practical as will be explained in the following. Thus all the 2N response functions are calculated as in Ref. [9], by direct integrations.

It is very important to realize that while the differential cross section  $\frac{d^3\sigma}{dE' d\Omega'}$  depends on three kinematical variables,  $E$ ,  $\theta$ , and  $E'$ , the response functions are defined in terms of the internal nuclear energy  $E_{\text{c.m.}}$  and the magnitude of the three-momentum transfer  $Q$ . We will use this feature to facilitate the calculations.

We follow the path paved by Refs. [3–6], whose authors investigated inclusive neutrino scattering on the deuteron with configuration space methods. Those very advanced investigations were performed with traditional and chiral NN potentials and included weak nuclear current operators with one- and two-body contributions, the latter adjusted to the NN force. Here we continue our work from Ref. [9] with the AV18

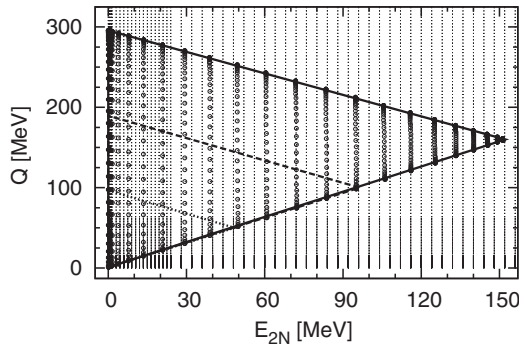


FIG. 1. Rectilinear grid of  $(E_{2N}, Q)$  points used to store the response functions for the  $\bar{\nu}_e + {}^2\text{H} \rightarrow e^- + p + p$  reaction (tiny dots) and the actual  $(E_{2N}, Q)$  points used to evaluate the total cross section (circles) in the triangle-like area for the initial neutrino energy  $E = 160$  MeV. Border lines for two smaller energies, 50 and 100 MeV, are also shown.

NN potential [8] and the single-nucleon current operator defined in Ref. [15], previously employed, for example, in Refs. [11,15]. Since we restrict ourselves to low (anti)neutrino energies,  $E \leq 160$  MeV, we expect, based on the results of

Ref. [5], that 2N contributions in the current operators would lead to effects smaller than 2–4%. Our expectation can be further supported by the very recent results for the cross sections in inclusive neutrino scattering off the deuteron that were calculated by Baroni and Schiavilla in Ref. [6] for essentially the same range of initial (anti)neutrino energies but in a chiral effective field theory framework. The authors included higher order terms (up to N4LO) to the 2N weak current operator but found small effects of these contributions beyond the leading order. Their results were quite close (systematically larger by approximately 2%) to the earlier predictions of Ref. [4] using semiphenomenological NN forces and related current operators. Taking into account the findings of Refs. [6,9], we can consider our predictions for the 3N reactions to be quite reliable, albeit clearly leaving room for improvement.

### III. RESULTS FOR (ANTI)NEUTRINO SCATTERING ON ${}^2\text{H}$

Calculating the total cross section for (anti)neutrino induced breakup reactions for many initial (anti)neutrino energies, starting for each energy anew, could lead in fact to a waste of computer resources. As we show in Fig. 1 for the  $\bar{\nu}_e + {}^2\text{H} \rightarrow e^- + p + p$  reaction, while calculating the total

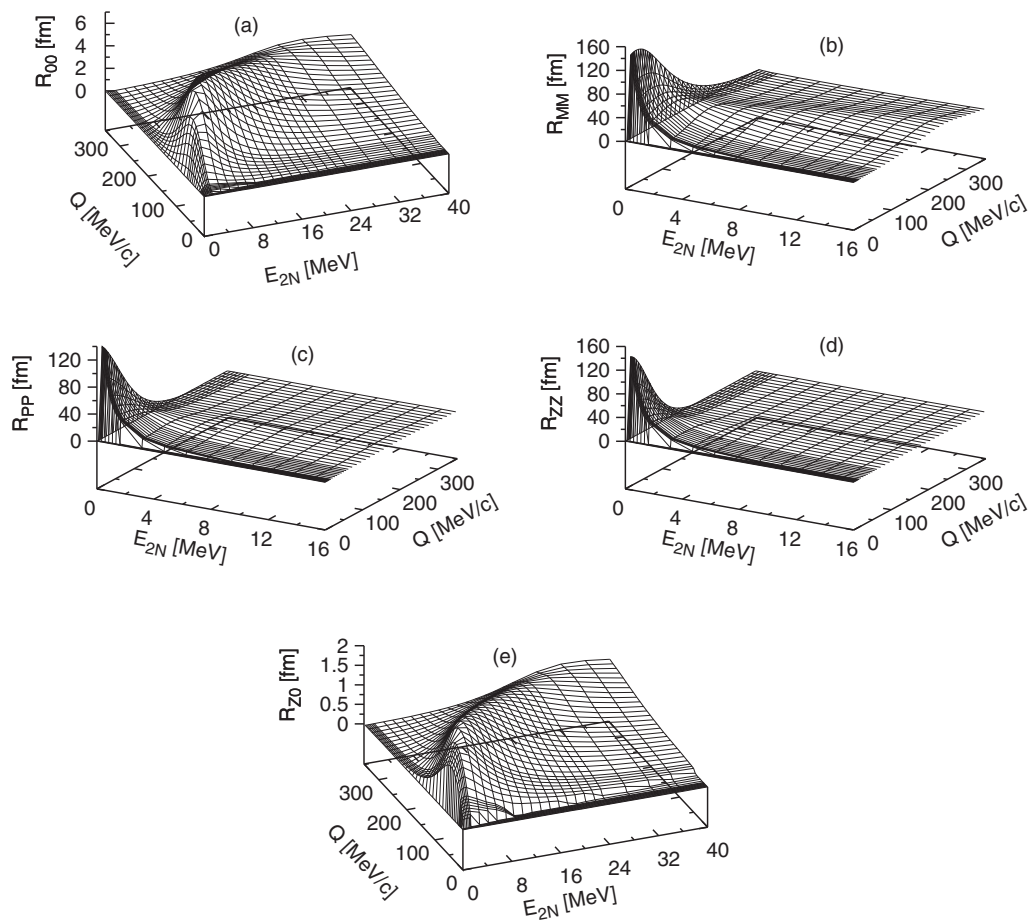


FIG. 2. Nuclear inclusive response functions  $R_{00}$  (a),  $R_{MM}$  (b),  $R_{PP}$  (c),  $R_{ZZ}$  (d), and  $R_{Z0}$  (e) for the  $\bar{\nu}_e + {}^2\text{H} \rightarrow e^+ + n + n$  reaction as a function of the internal 2N energy  $E_{2N}$  and the magnitude of the three-momentum transfer  $Q$ . The results are obtained with the AV18 NN potential and the single-nucleon CC operator, which contains the relativistic corrections, employing the nonrelativistic kinematics.

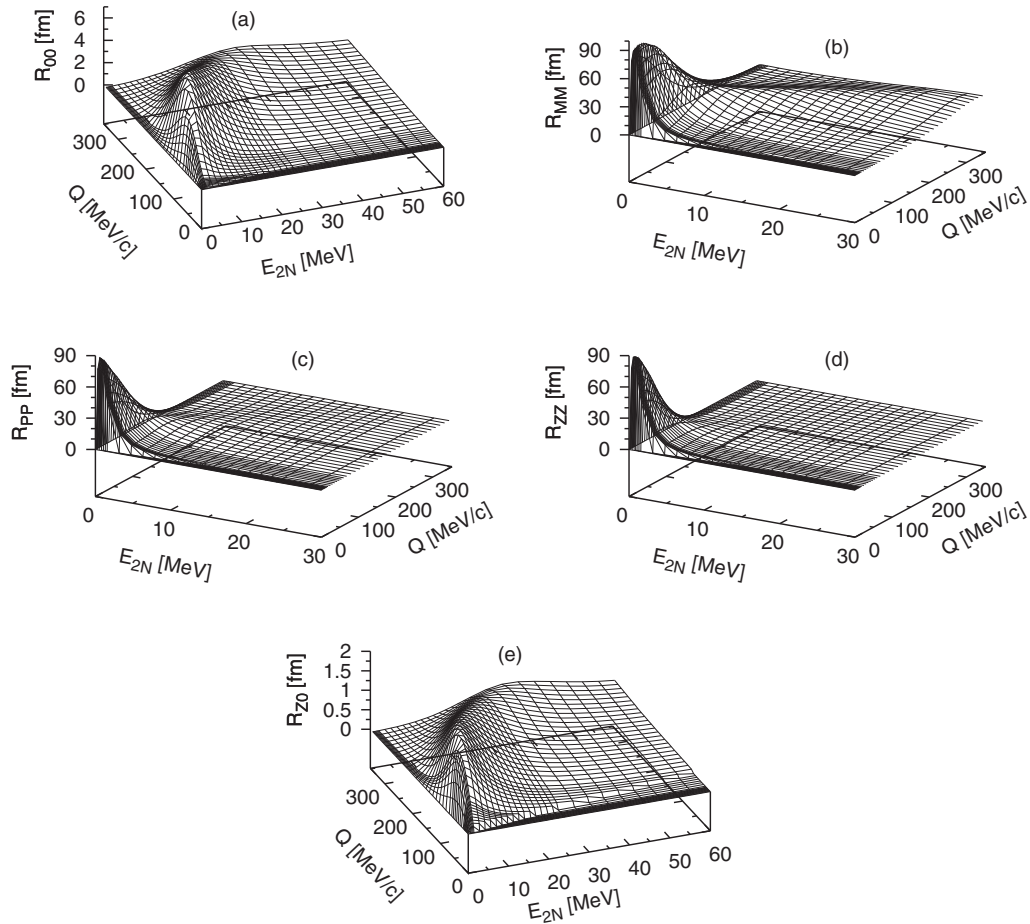


FIG. 3. Same as Fig. 2, but for the  $\nu_e + {}^2\text{H} \rightarrow e^- + p + p$  reaction.

cross section for increasing initial antineutrino energies, the dynamical information in the form of response functions is taken from a part of the  $(E_{2N}, Q)$  domain, which necessarily overlaps with the region corresponding to lower energies. This is also true for the reactions with the trinucleons. That is why calculating response functions on a sufficiently dense grid and using stored values for interpolations to integral  $(E_{2N}, Q)$  points appears to be advantageous. The same stored response functions can be used not only to generate the total cross sections but also to calculate the intermediate differential cross sections  $d^3\sigma/(dE' d\Omega')$  and  $d\sigma/d\theta$ . Yet another advantage of storing response functions becomes clear for the NC induced processes, where *the same* response functions are used for the neutrino and antineutrino induced reactions.

Before embarking on 3N calculations, this approach was tested in the 2N system, where results of the direct calculations of the total cross sections as defined, for example, in Eq. (2.22) of Ref. [9] and predictions based on the response function interpolations could be easily compared. The various sets of response functions should be prepared with great care, taking into account the character of their dependence on  $E_{2N}$  and  $Q$ . We decided to use simple rectilinear grids, which forced us to use many points on the whole grid, even if a sharp maximum was strongly localized, leading, however, to

very accurate predictions. This feature of our calculations is clearly visible in Fig. 1.

In Figs. 2–4 we show the three sets of the response functions obtained for the  $\bar{\nu}_e + {}^2\text{H} \rightarrow e^+ + n + n$ ,  $\nu_e + {}^2\text{H} \rightarrow e^- + p + p$ , and  $\nu_e(\bar{\nu}_e) + {}^2\text{H} \rightarrow \nu_e(\bar{\nu}_e) + p + n$  reactions. We use different  $E_{2N}$  and  $Q$  ranges in the figures to display the particular features of the response functions. Note that the figures are *not* drawn with all calculated points, so the actual grids for two-dimensional interpolations are in fact much denser. All the response functions have a maximum in the vicinity of the  $(0,0)$  point but their shapes and heights are very different. The response functions  $R_{00}$  and  $R_{Z0}$  originating at least partly from the  $N^0$  nuclear matrix elements are, for all three reactions, dwarfed by the response functions  $R_{MM}$ ,  $R_{PP}$ , and  $R_{ZZ}$ , which are by two orders of magnitude more pronounced. Note that for each  $E_{2N} > 0$  there is an interval  $[0, Q_{\min}]$  which cannot be physically realized for any initial neutrino energy and for which the values of the response functions are simply set to zero.

From the response functions it is straightforward to compute the differential and total cross sections. To this end one interpolates the response functions in two dimensions over the  $(E_{2N}, Q)$  grid points to the particular  $(\bar{E}_{2N}, \bar{Q})$  value resulting from the  $(E, \theta, E')$  set. We used three different methods to interpolate the response functions. While the first two

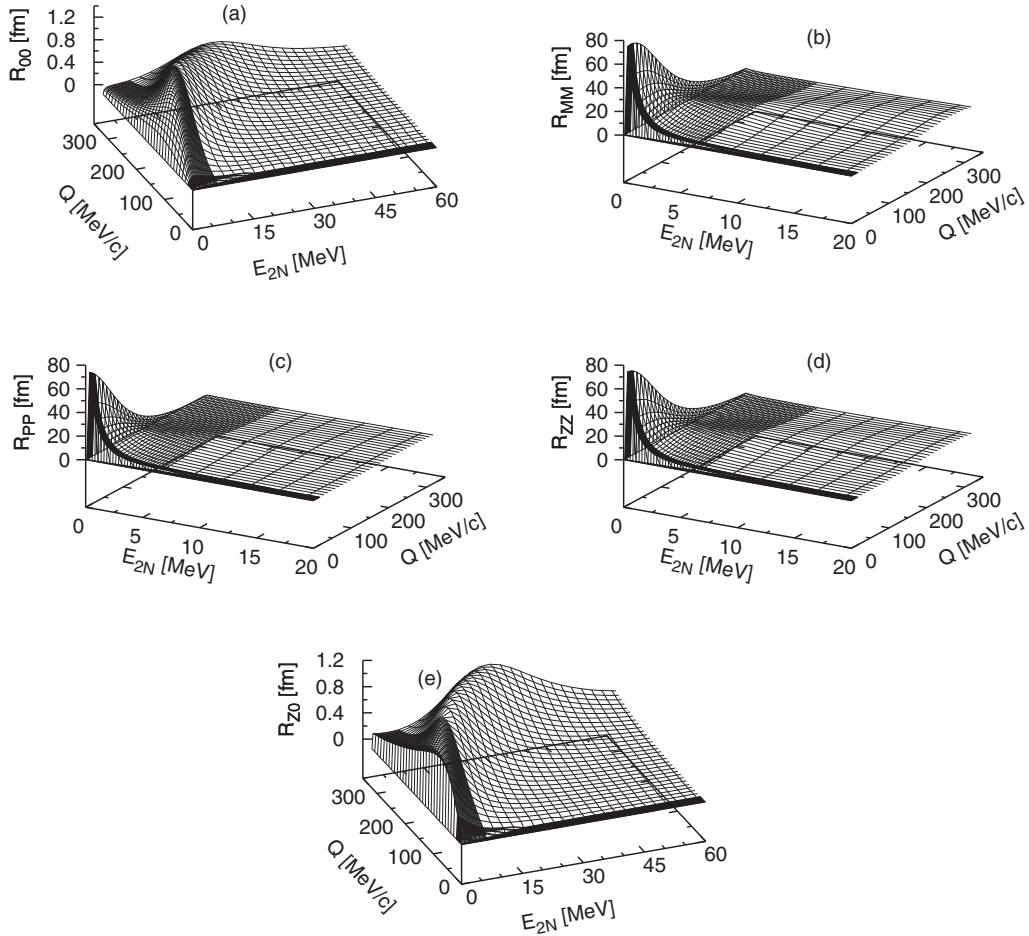


FIG. 4. Same as Figs. 2 and 3, but for the weak NC driven  $\bar{\nu}_e + {}^2\text{H} \rightarrow \bar{\nu}_e + p + n$  and  $\nu_e + {}^2\text{H} \rightarrow \nu_e + p + n$  reactions.

methods employed consecutive cubic spline (from Ref. [30] or Ref. [31]) interpolations, first along the  $Q$  direction and then along the  $E_{2N}$  direction, the third method was a straightforward bilinear interpolation. In this way we could control the quality of interpolations, since we required that results for all considered observables, obtained by the three methods, did not deviate from the average by more than 1%. Additional

points were added to the grid, when that criterion was not met. Since the 2N calculations are relatively easy, we could consider grids that contained from 7200 to 17 200 points. This procedure was especially important for the 3N case, where we did not calculate cross sections directly but fully relied on response function interpolations. In the following we show results based on the interpolation scheme from Ref. [30].

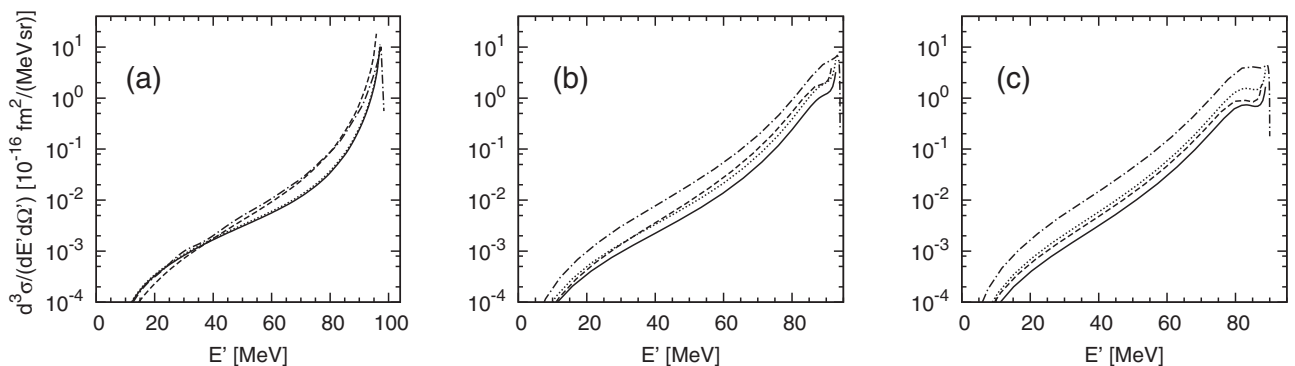


FIG. 5. Triple differential cross section  $d^3\sigma / (dE' d\Omega')$  for the  $\bar{\nu}_e + {}^2\text{H} \rightarrow e^+ + n + n$  (dashed line),  $\nu_e + {}^2\text{H} \rightarrow e^- + p + p$  (dash-dotted line),  $\bar{\nu}_e + {}^2\text{H} \rightarrow \bar{\nu}_e + p + n$  (solid line), and  $\nu_e + {}^2\text{H} \rightarrow \nu_e + p + n$  (dotted line) reactions for the initial (anti)neutrino energy  $E = 100$  MeV at three laboratory scattering angles:  $\theta = 27.5^\circ$  (a),  $\theta = 90^\circ$  (b), and  $\theta = 152.5^\circ$  (c) as a function of the final lepton energy  $E'$ . The results are obtained with the AV18 potential and with the single-nucleon current, employing the nonrelativistic kinematics.

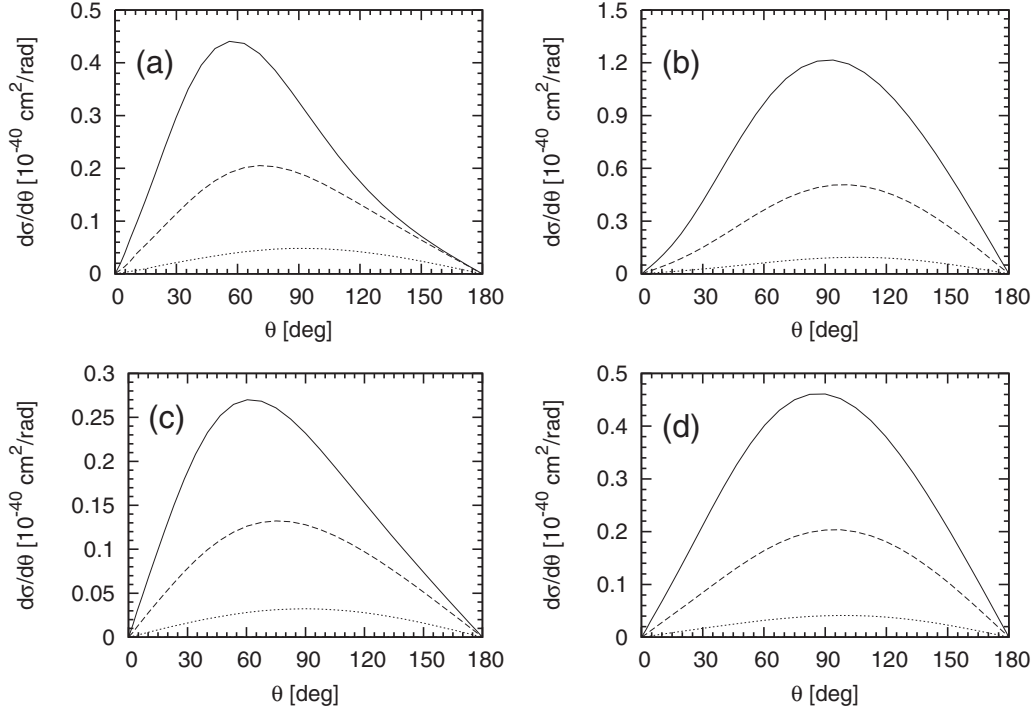


FIG. 6. Differential cross section  $d\sigma/d\theta$  for the  $\bar{\nu}_e + {}^2\text{H} \rightarrow e^+ + n + n$  (a),  $\nu_e + {}^2\text{H} \rightarrow e^- + p + p$  (b),  $\bar{\nu}_e + {}^2\text{H} \rightarrow \bar{\nu}_e + p + n$  (c), and  $\nu_e + {}^2\text{H} \rightarrow \nu_e + p + n$  (d) reactions as a function of the laboratory scattering angle  $\theta$  for initial (anti)neutrino energy  $E = 50$  MeV (dotted line), 100 MeV (dashed line), and 150 MeV (solid line). The results are obtained with the AV18 potential and with the single-nucleon current, employing the nonrelativistic kinematics.

The triple differential cross section,  $d^3\sigma/(dE' d\Omega')$ , for a fixed lepton scattering angle is a function of the final lepton energy  $E'$ . In Fig. 5 we show examples of such cross sections for the initial (anti)neutrino energy  $E = 100$  MeV and for three different lepton scattering angles  $\theta = 27.5^\circ$ ,  $\theta = 90^\circ$ , and  $\theta = 152.5^\circ$ . These results can be compared with the middle panels of Figs. 6 and 9 in Ref. [5] and show that the cross sections rise very rapidly with the final (anti)lepton energy, changing in the allowed energy range by several orders of magnitude.

For all four studied reactions we show also in Fig. 6 the angular distributions of the cross sections,  $d\sigma/d\theta$ , which are given as

$$\frac{d\sigma}{d\theta} = 2\pi \sin\theta \int_{(E')_{\min}}^{(E')_{\max}} dE' \frac{d^3\sigma}{dE' d\Omega'}, \quad (3.1)$$

where  $(E')_{\min} = M_e(0)$  for the CC (NC) induced reactions and the factor  $2\pi$  arises from the integration over the azimuthal angle  $\phi$ . Clearly, the angular distributions rise with the incident energy. For the smallest  $E = 50$  MeV they are all almost symmetric with respect to  $\theta = 90^\circ$ . This symmetry is roughly preserved for the higher energies  $E = 100$  and 150 MeV in the case of the two neutrino induced reactions, but for the two other reactions the angular distributions become asymmetric and their maxima are shifted toward forward angles. This behavior is most evident for the  $\bar{\nu}_e + {}^2\text{H} \rightarrow e^+ + n + n$  process.

By the final integration over the scattering angle  $\theta$  we arrive at the total cross section

$$\sigma_{\text{tot}} = \int_0^\pi d\theta \frac{d\sigma}{d\theta}. \quad (3.2)$$

These important observables were first presented in Refs. [3–6] and our momentum space based results shown in

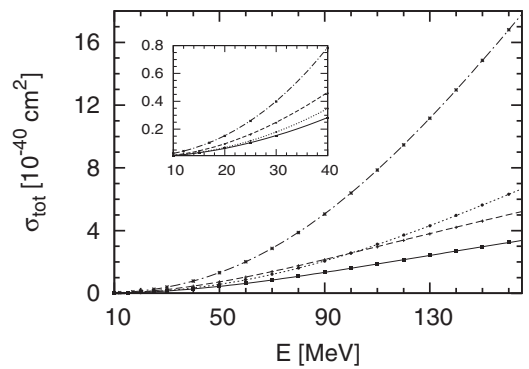


FIG. 7. Total cross section  $\sigma_{\text{tot}}$  for the  $\bar{\nu}_e + {}^2\text{H} \rightarrow e^+ + n + n$  (dashed line),  $\nu_e + {}^2\text{H} \rightarrow e^- + p + p$  (dash-dotted line),  $\bar{\nu}_e + {}^2\text{H} \rightarrow \bar{\nu}_e + p + n$  (solid line), and  $\nu_e + {}^2\text{H} \rightarrow \nu_e + p + n$  (dotted line) reactions as a function of the initial (anti)neutrino energy  $E$  calculated directly [9] (symbols) or from the interpolated response functions (lines) as explained in the text. The results are obtained with the AV18 potential and with the single-nucleon current, employing the nonrelativistic kinematics. The inset focuses on the results for  $E \leq 40$  MeV.

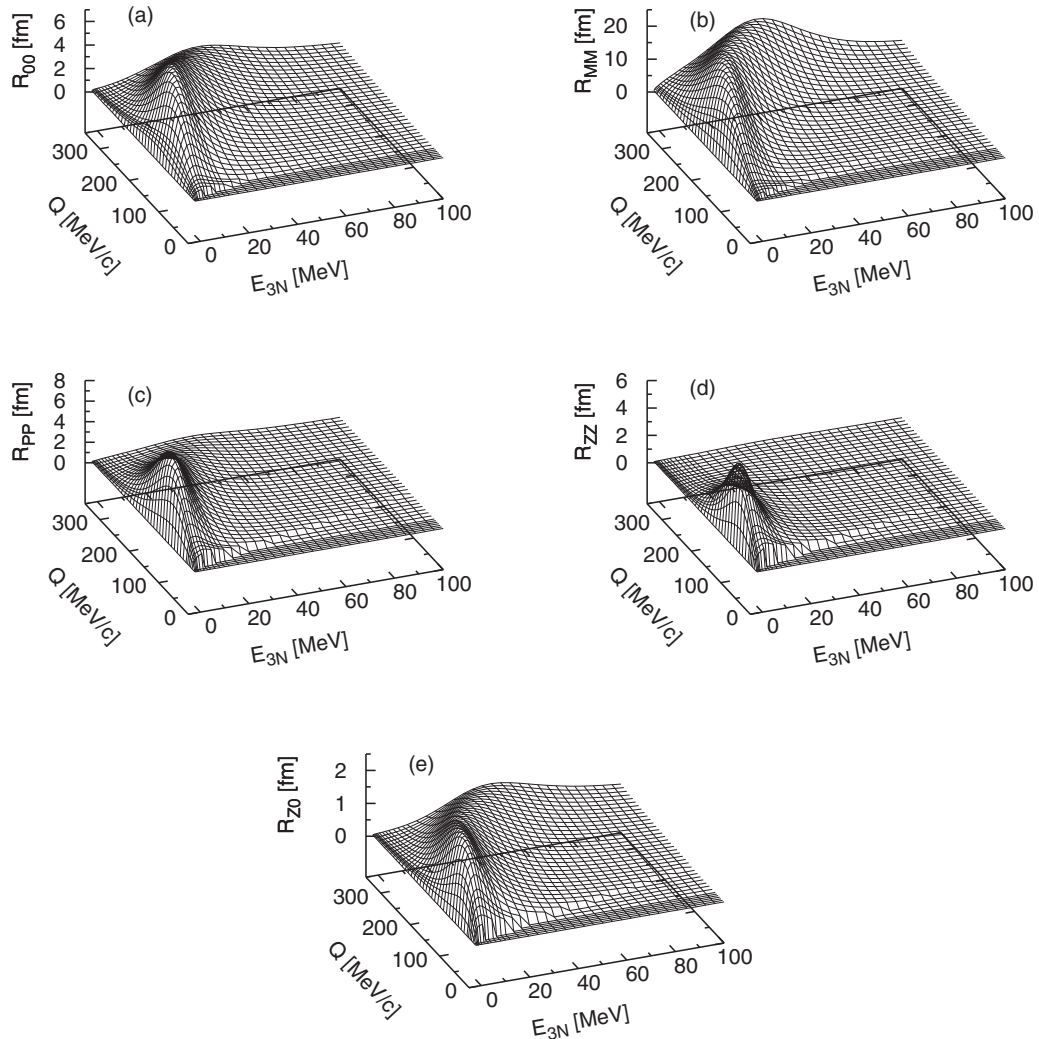


FIG. 8. Total inclusive CC response functions  $R_{00}$  (a),  $R_{MM}$  (b),  $R_{PP}$  (c),  $R_{ZZ}$  (d), and  $R_{Z0}$  (e) for the CC electron antineutrino disintegration of  ${}^3\text{He}$  as a function of the internal 3N energy  $E_{3N}$  and the magnitude of the three-momentum transfer  $Q$ . The results are obtained with the AV18 NN potential and the single-nucleon CC operator, which contains the relativistic corrections.

Figs. 2 and 4 of Ref. [9] agreed very well with the predictions presented in Ref. [5]. Despite the distinct treatment of kinematics the differences for none of the reactions for  $E \leq 150$  MeV exceed 2% for the single-nucleon current calculations and 6% for calculations including additionally two-nucleon currents. In Fig. 7 we display a comparison of directly obtained results for the total cross sections from Ref. [5] with the predictions based on the response function interpolations. The agreement is very good for all four reactions and for all considered (anti)neutrino energies, justifying our “economical” approach to calculations of the cross sections.

#### IV. RESULTS FOR (ANTI)NEUTRINO SCATTERING ON ${}^3\text{He}$ AND ${}^3\text{H}$

We follow the same path for the trinucleons as for the calculations with the deuteron target. That means that also in this case we calculate the response functions on a grid of

$(E_{3N}, Q)$  points. As already mentioned, one can evaluate the response functions by introducing explicit integrations over the available phase space, in particular differentiating between the two- and three-body reaction channels. It is also possible to evaluate the response functions without any resort to explicit final-state kinematics [9,28,29]. These two approaches were used and compared successfully in Ref. [9] for a small number of  $(E_{3N}, Q)$  points. Since we wanted to produce full grids of response functions, we decided to employ the second scheme. Each 3N grid comprised roughly 2000 points. Even if some points on the rectilinear grids lied in the nonphysical region, where no calculations are necessary and where the response functions are just zero, the actual number of the computations was high. In order to efficiently deal with so many calculations, we prepared a special computational framework based on functional programming and algebraic types to distribute the calculations among several desktop computers. Our calculations were performed with the AV18 NN potential, neglecting the 3N force, and with the same

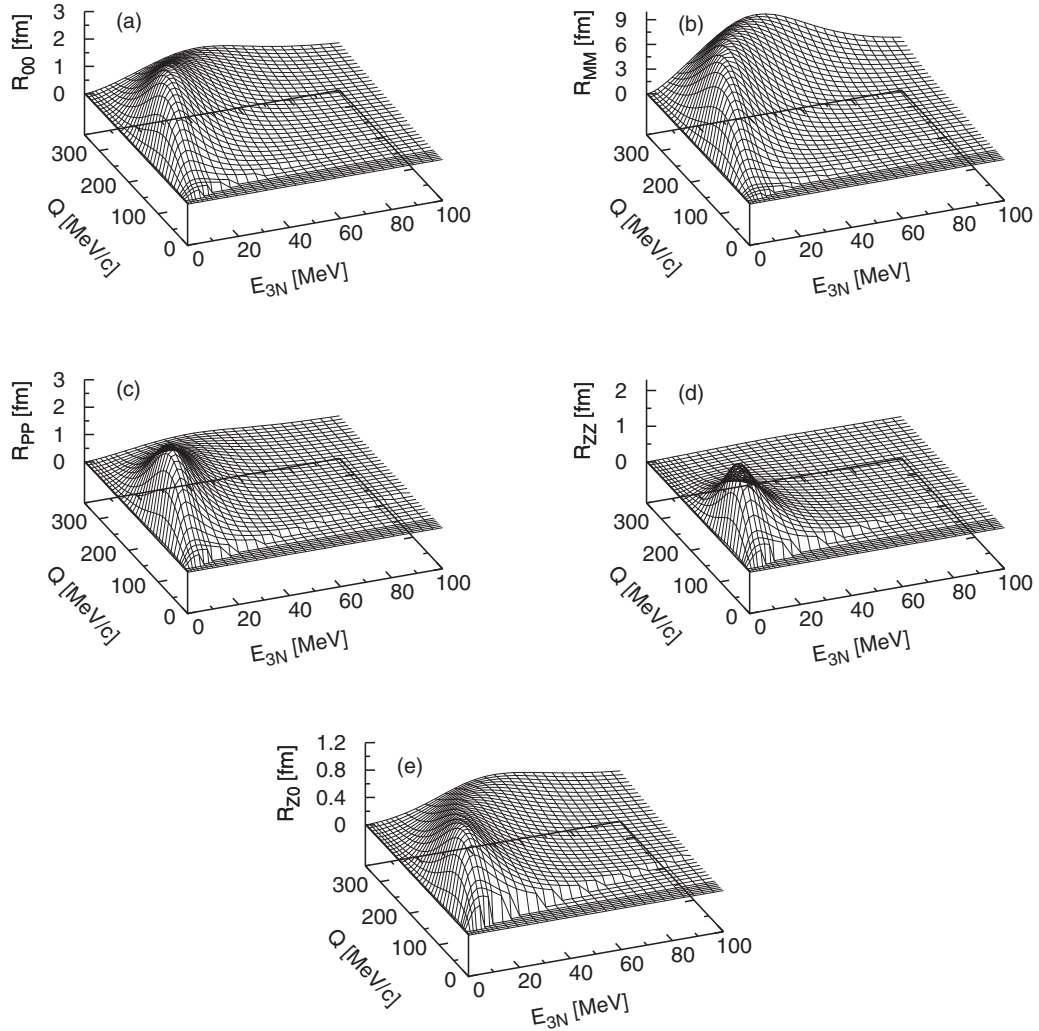


FIG. 9. Same as Fig. 8, but for the  $\bar{\nu}_e + {}^3\text{H} \rightarrow e^+ + n + n + n$  reaction.

single-nucleon current as in the 2N case. Since we do not include the proton-proton Coulomb force for the 3N scattering states, for the CC driven reactions we restricted ourselves to the antineutrino induced reactions, which reduce the nuclear charge. We investigated also the NC reactions on  ${}^3\text{He}$  and  ${}^3\text{H}$ , although we are aware that our predictions for the weak NC response functions of  ${}^3\text{He}$  might prove inaccurate for some parts of the phase space, where the proton-proton Coulomb force becomes important. The strongest Coulomb repulsion effects can be expected for low relative proton-proton energies. It is difficult to estimate the size of the neglected Coulomb force effects on these observables. Our approach is, however, at least partly justified by a reasonable agreement between the data and analogous theoretical predictions for the inclusive response functions in electron scattering on  ${}^3\text{He}$  [29].

We start presenting our results with the 3N weak response functions, shown in Figs. 8–11. Note that Figs. 8, 9 and 10 in Ref. [9] are just cross sections for  $Q = 100/c$  MeV through the three-dimensional plots given here in Figs. 8, 11, and 10, respectively. It is clear that the 3N response functions are

much broader and extend toward higher  $E_{3N}$  and  $Q$  values than the corresponding 2N observables, which are very localized. The differences between various response functions are not so strong as in the 2N case. The response functions for the CC electron antineutrino disintegration of  ${}^3\text{He}$  and  ${}^3\text{H}$  (Figs. 8 and 9) have similar shapes and roughly scale according to the number of protons in a nucleus. This seems to reflect the fact that the process described by the single-nucleon current involves only protons.

In the case of the NC response functions the proton and neutron contributions to the single nucleon NC operator are comparable. This leads to similar results for the  ${}^3\text{He}$  and  ${}^3\text{H}$  NC response functions displayed in Figs. 10–11.

As in the 2N cases, the response functions are the key ingredients of the cross sections, where only total or partial information about the final lepton is retained. The triple differential cross section  $d^3\sigma/(dE' d\Omega')$  for the CC electron antineutrino disintegration, NC electron antineutrino disintegration, and NC electron neutrino disintegration of  ${}^3\text{He}$  just for one initial (anti)neutrino energy  $E = 100$  MeV at three scattering angles  $\theta = 27.5^\circ$ ,  $\theta = 90^\circ$ , and  $\theta = 152.5^\circ$



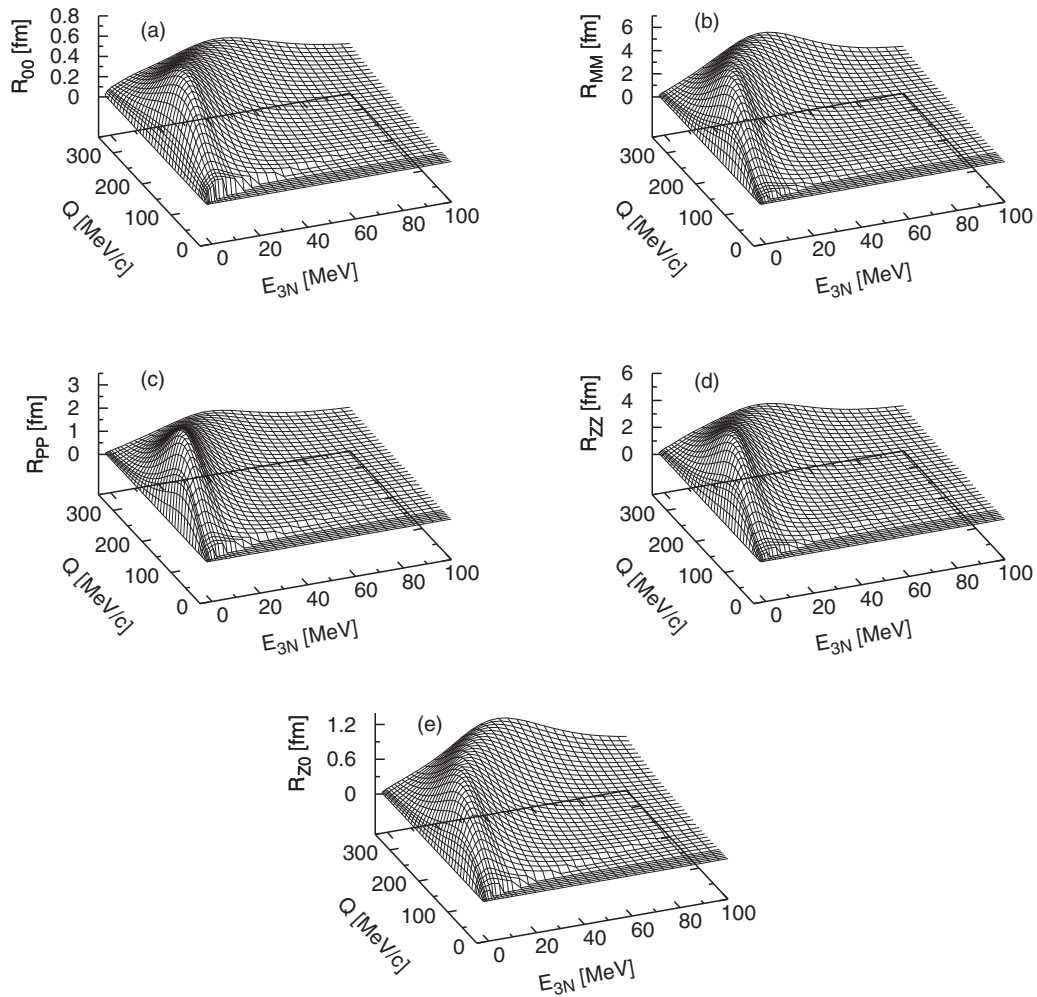


FIG. 10. Same as Figs. 8 and 9, but for inclusive NC response functions for (anti)neutrino disintegration of  ${}^3\text{He}$ .

are displayed in Fig. 12 as a function of the final lepton energy  $E'$ . All the cross sections soar with increasing  $E'$  and they are pulled down only in the vicinity of  $(E')_{\text{max}}$ . At the selected forward angle the cross section for the CC driven process assumes the highest values and the results for the NC reactions with antineutrinos and neutrinos nearly overlap (at least observed on the logarithmic scale). For the two other values of  $\theta$  the antineutrino and neutrino NC cross sections are clearly separated and the cross section for the neutrino induced NC breakup of  ${}^3\text{He}$  is quite close to the prediction for the antineutrino induced CC process.

The corresponding predictions for the same reactions on  ${}^3\text{H}$  are shown in Fig. 13. At  $\theta = 27.5^\circ$  the cross section for the CC reaction dominates for  $40 < E' < 85$  MeV but not over the whole  $E'$  interval. For  $\theta = 90^\circ$  and  $\theta = 152.5^\circ$  the cross section for the neutrino induced NC breakup of  ${}^3\text{H}$  assumes higher values than the other two cross sections.

We give only sample results but it is clear that similar calculations can be used to plan experimental investigations of the NC and CC (anti)neutrino induced reactions.

As a last step before discussing the total cross section, we show in Fig. 14 the six angular distributions of the cross sections, which can be now easily obtained from the

response functions. We do it again for the same incoming (anti)neutrino energies as in Fig. 6 for the reactions on the deuteron. The curves are less symmetric compared to the predictions from Fig. 6, which is clearly visible for the two higher  $E$  values. There is a clear similarity between the results shown in Figs. 14(a) and 14(b) for the antineutrino induced CC processes on  ${}^3\text{He}$  and  ${}^3\text{H}$ , which can be traced back to the scaling properties of the corresponding response functions. For the highest energy  $E = 150$  MeV the maxima for all the cross sections with antineutrinos are shifted toward forward angles; only for the neutrino induced NC processes displayed in Figs. 14(d) and 14(f) the maxima are reached for  $\theta > 90^\circ$ .

Finally we arrive at the most important results: the total cross sections for the studied (anti)neutrino reactions with the trinucleons. They can be found in Fig. 15 for  ${}^3\text{He}$  and in Fig. 16 for  ${}^3\text{H}$ . In the  ${}^3\text{He}$  case the cross section for CC electron antineutrino disintegration takes the highest values in the whole investigated energy range. It is followed by the cross section for NC electron neutrino disintegration. The cross section for NC electron antineutrino disintegration is approximately two times smaller than the cross section for the corresponding CC driven process.

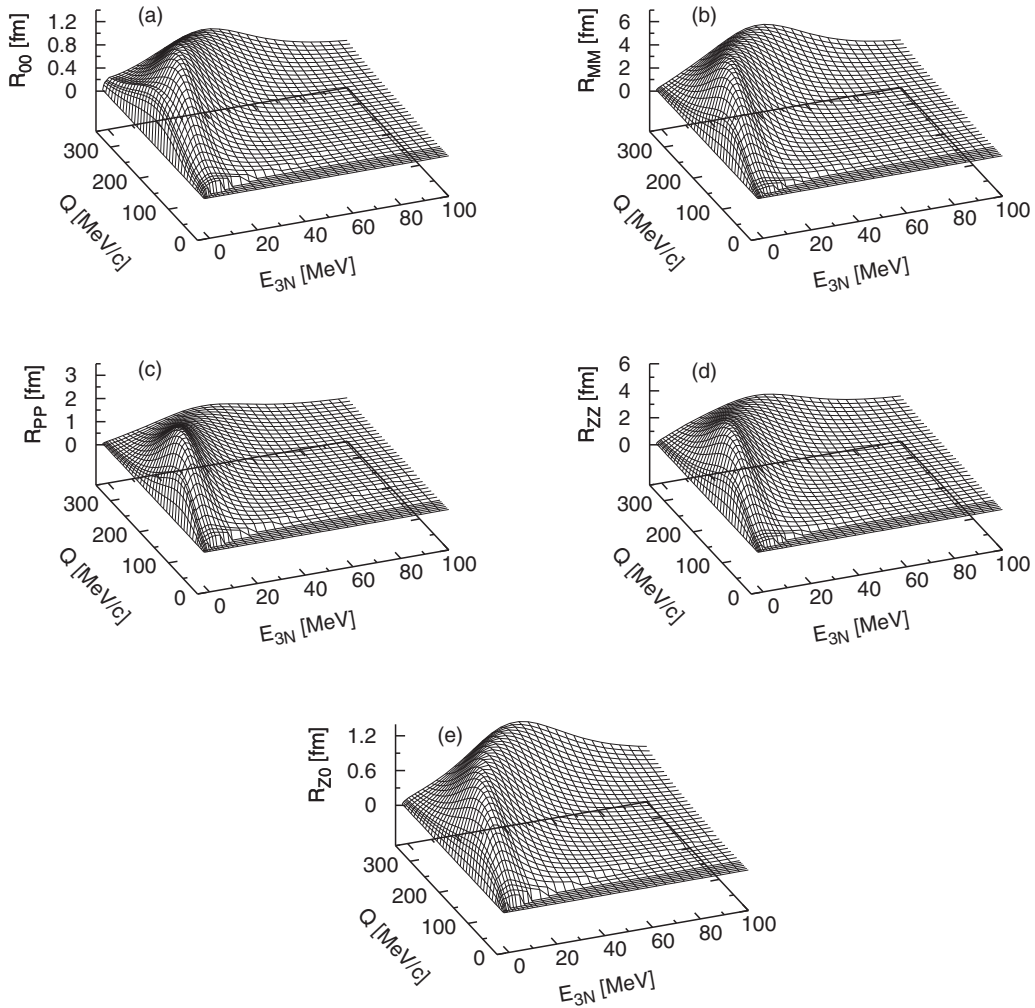


FIG. 11. Same as Fig. 10, but for  ${}^3\text{H}$ .

The picture is different for  ${}^3\text{H}$ , where the cross section for NC electron neutrino disintegration is roughly two times larger than the predictions for the two antineutrino induced reactions, which are close to each other for all the initial (anti)neutrino energies.

### V. SUMMARY

We extended our studies of (anti)neutrino scattering off the deuteron and trinucleons from Ref. [9], where we presented our momentum space framework and obtained predictions for the total cross sections only for the reactions on the deuteron.

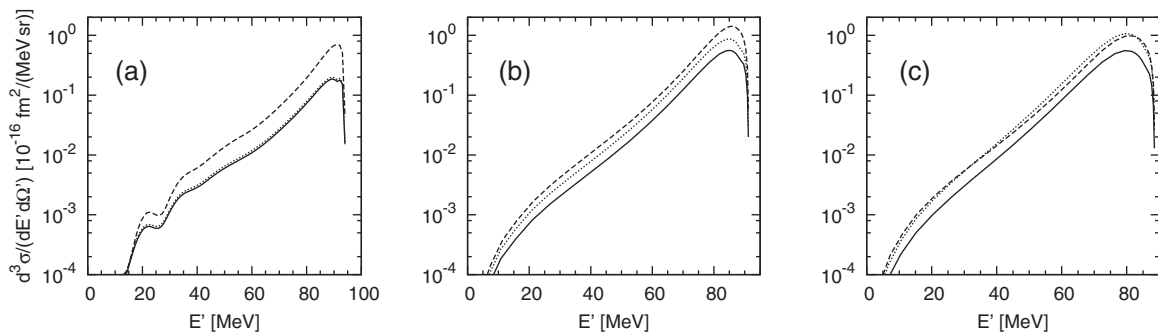
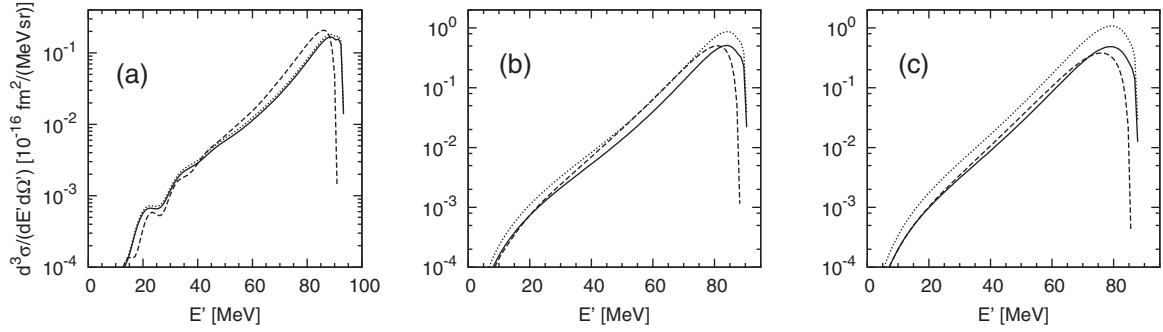


FIG. 12. Triple differential cross section  $d^3\sigma/(dE' d\Omega')$  for the CC electron antineutrino disintegration of  ${}^3\text{He}$  (dashed line), NC electron antineutrino disintegration of  ${}^3\text{He}$  (solid line), and NC electron neutrino disintegration of  ${}^3\text{He}$  (dotted line) for the initial (anti)neutrino energy  $E = 100$  MeV at three laboratory scattering angles:  $\theta = 27.5^\circ$  (a),  $\theta = 90^\circ$  (b), and  $\theta = 152.5^\circ$  (c) as a function of the final lepton energy  $E'$ . The results are obtained with the AV18 potential and with the single-nucleon current, employing the nonrelativistic kinematics.

FIG. 13. Same as Fig. 12, but for the reactions on  ${}^3\text{H}$ .

For the reactions on the trinucleons we could perform only feasibility studies in Ref. [9], employing two different methods to calculate the essential response functions. In the present paper we provide full information about the cross sections for CC electron antineutrino disintegration, NC electron antineu-

trino disintegration, and NC electron neutrino disintegration of  ${}^3\text{He}$  and  ${}^3\text{H}$ .

The material presented in this paper is based on tens of thousands of 2N and several thousand 3N scattering calculations, which were necessary to fill dense two-dimensional

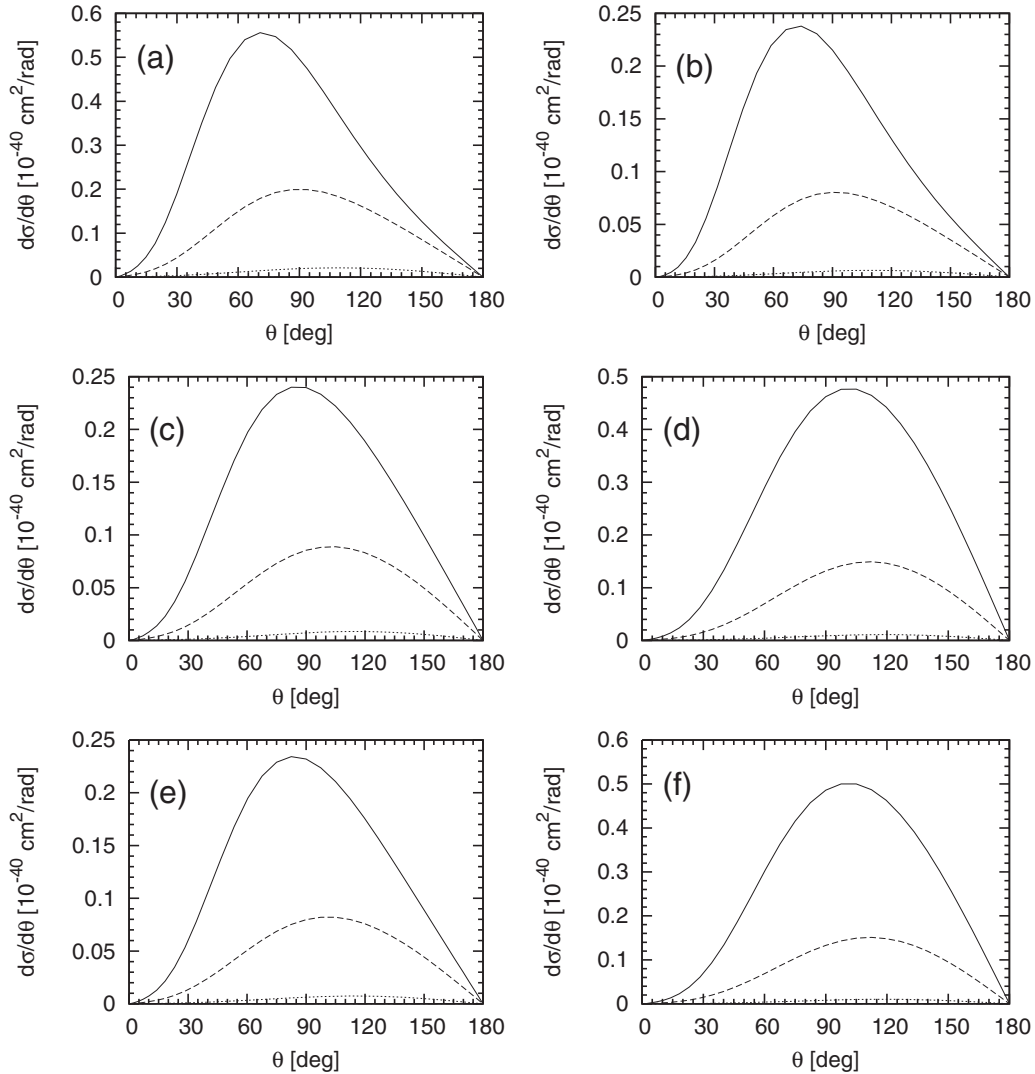


FIG. 14. Same as Fig. 6, but for the inclusive CC electron antineutrino disintegration of  ${}^3\text{He}$  (a), CC electron antineutrino disintegration of  ${}^3\text{H}$  (b), NC electron antineutrino disintegration of  ${}^3\text{He}$  (c), NC electron neutrino disintegration of  ${}^3\text{He}$  (d), NC electron antineutrino disintegration of  ${}^3\text{H}$  (e), and NC electron neutrino disintegration of  ${}^3\text{H}$  (f).

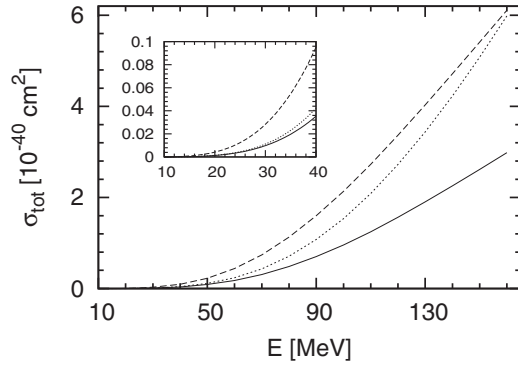


FIG. 15. Same as Fig. 7, but for three inclusive (anti)neutrino reactions with  ${}^3\text{He}$ : CC electron antineutrino disintegration of  ${}^3\text{He}$  (dashed line), NC electron antineutrino disintegration of  ${}^3\text{He}$  (solid line), and NC electron neutrino disintegration of  ${}^3\text{He}$  (dotted line).

grids, from which essentially in no time other observables (threefold differential cross sections, angular distributions of the cross sections, and, most importantly, the total cross sections) can be obtained. The results of our calculations in the form of the tabulated response functions are available to the interested reader. This whole procedure was first carefully tested for the reactions on the deuteron, where the observables had been calculated directly and where accurate predictions obtained in coordinate space were available.

Our calculations leave room for improvement: they have been performed with the single-nucleon current operator and without a 3N force, neglecting additionally the Coulomb force between two final protons for one of the studied reactions. Nevertheless our predictions are obtained with the fully realistic AV18 nucleon-nucleon potential [8] and are restricted to the (anti)neutrino energy region, where two-nucleon current and 3N force effects are not expected to be very important and should not exceed 10%. Thus we provide important information about (anti)neutrino interactions with very light nuclei.

A consistent framework for the calculations of neutrino induced processes on  ${}^2\text{H}$ ,  ${}^3\text{He}$ ,  ${}^3\text{H}$ , and other light nuclei

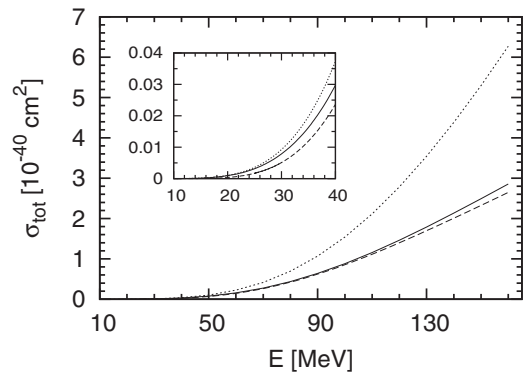


FIG. 16. Same as Fig. 15, but for three inclusive (anti)neutrino reactions with  ${}^3\text{H}$ .

is still a challenge, despite the recent progress in this field. There are many models of the nuclear interactions and weak current operators linked to these forces, but full compatibility has not been achieved yet. We hope that the work on the regularization of the 2N and 3N chiral potentials as well as consistent electroweak current operators will be completed in the near future. This will allow us to repeat the calculations of the response functions and related observables within a better dynamical framework. We believe, however, that the results presented in this paper constitute an important step toward a consistent framework for the calculation of several neutrino induced processes on  ${}^2\text{H}$ ,  ${}^3\text{He}$ ,  ${}^3\text{H}$ , and other light nuclei.

## ACKNOWLEDGMENTS

This work is a part of the LENPIC project and was supported by the Polish National Science Centre under Grants No. 2016/22/M/ST2/00173 and No. 2016/21/D/ST2/01120. The numerical calculations were partially performed on the supercomputer cluster of the JSC, Jülich, Germany.

- 
- [1] O. Benhar, P. Huber, C. Mariani, and D. Meloni, *Phys. Rep.* **700**, 1 (2017).
- [2] L. Alvarez-Ruso *et al.*, *Prog. Part. Nucl. Phys.* **100**, 1 (2018).
- [3] S. Nakamura, T. Sato, V. Gudkov, and K. Kubodera, *Phys. Rev. C* **63**, 034617 (2001); **73**, 049904(E) (2006).
- [4] S. Nakamura *et al.*, *Nucl. Phys. A* **707**, 561 (2002).
- [5] G. Shen, L. E. Marcucci, J. Carlson, S. Gandolfi, and R. Schiavilla, *Phys. Rev. C* **86**, 035503 (2012).
- [6] A. Baroni and R. Schiavilla, *Phys. Rev. C* **96**, 014002 (2017).
- [7] J. Carlson and R. Schiavilla, *Rev. Mod. Phys.* **70**, 743 (1998).
- [8] R. B. Wiringa, V. G. J. Stoks, and R. Schiavilla, *Phys. Rev. C* **51**, 38 (1995).
- [9] J. Golak, R. Skibiński, K. Topolnicki, H. Witała, A. Grassi, H. Kamada, and L. E. Marcucci, *Phys. Rev. C* **98**, 015501 (2018).
- [10] D. Gazit, *Phys. Lett. B* **666**, 472 (2008).
- [11] L. E. Marcucci, M. Piarulli, M. Viviani, L. Girlanda, A. Kievsky, S. Rosati, and R. Schiavilla, *Phys. Rev. C* **83**, 014002 (2011).
- [12] L. E. Marcucci, A. Kievsky, S. Rosati, R. Schiavilla, and M. Viviani, *Phys. Rev. Lett.* **108**, 052502 (2012); **121**, 049901(E) (2018).
- [13] L. E. Marcucci, R. Schiavilla, and M. Viviani, *Phys. Rev. Lett.* **110**, 192503 (2013); **123**, 019901(E) (2019).
- [14] L. E. Marcucci and R. Machleidt, *Phys. Rev. C* **90**, 054001 (2014).
- [15] J. Golak, R. Skibiński, H. Witała, K. Topolnicki, A. E. Elmeshneeb, H. Kamada, A. Nogga, and L. E. Marcucci, *Phys. Rev. C* **90**, 024001 (2014).
- [16] J. Golak, R. Skibiński, H. Witała, K. Topolnicki, H. Kamada, A. Nogga, and L. E. Marcucci, *Phys. Rev. C* **94**, 034002 (2016).

- [17] A. Baroni, L. Girlanda, A. Kievsky, L. E. Marcucci, R. Schiavilla, and M. Viviani, *Phys. Rev. C* **94**, 024003 (2016); **95**, 059902(E) (2017).
- [18] S. L. Mintz, G. M. Gerstner, M. A. Barnett, and M. Pourkaviani, *Int. J. Mod. Phys. E* **8**, 197 (1999).
- [19] D. Gazit and N. Barnea, *Phys. Rev. C* **70**, 048801 (2004).
- [20] D. Gazit and N. Barnea, *Phys. Rev. Lett.* **98**, 192501 (2007).
- [21] E. O'Connor, D. Gazit, C. J. Horowitz, A. Schwenk, and N. Barnea, *Phys. Rev. C* **75**, 055803 (2007).
- [22] D. Efros, W. Leidemann, and G. Orlandini, *Phys. Lett. B* **338**, 130 (1994).
- [23] A. Lovato, S. Gandolfi, J. Carlson, S. C. Pieper, and R. Schiavilla, *Phys. Rev. Lett.* **112**, 182502 (2014).
- [24] A. Lovato, S. Gandolfi, J. Carlson, S. C. Pieper, and R. Schiavilla, *Phys. Rev. C* **91**, 062501(R) (2015).
- [25] A. Lovato, S. Gandolfi, J. Carlson, Ewing Lusk, Steven C. Pieper, and R. Schiavilla, *Phys. Rev. C* **97**, 022502(R) (2018).
- [26] N. Rocco, C. Barbieri, O. Benhar, A. De Pace, and A. Lovato, *Phys. Rev. C* **99**, 025502 (2019).
- [27] J. D. Walecka, *Theoretical Nuclear and Subnuclear Physics* (Oxford University, Oxford, 1995).
- [28] S. Ishikawa, J. Góolak, H. Witała, H. Kamada, W. Glöckle, and D. Hüber, *Phys. Rev. C* **57**, 39 (1998).
- [29] J. Góolak, R. Skibiński, H. Witała, W. Glöckle, A. Nogga, and H. Kamada, *Phys. Rep.* **415**, 89 (2005).
- [30] W. Glöckle, G. Hasberg, and A. R. Neghabian, *Z. Phys. A* **305**, 217 (1982).
- [31] D. Hüber, H. Witała, A. Nogga, W. Glöckle, and H. Kamada, *Few-Body Syst.* **22**, 107 (1997).